Environmental Science Processes & Impacts

ROYAL SOCIETY OF CHEMISTRY

PAPER

View Article Online
View Journal | View Issue

Cite this: *Environ. Sci.: Processes Impacts*, 2025, **27**, 473

Optical properties and photobleaching of wildfire ashes aqueous extracts†

Frank Leresche, *[ab] Sarah J. Fischer, ‡[ab] Shelby Buckley §[ab] and Fernando L. Rosario-Ortiz [ab]

Wildfires can severely degrade soils and watersheds. Post-fire rain events can leach ashes and altered dissolved organic matter (DOM) into streams, impacting water quality and carbon biogeochemistry. The photochemical properties and persistence of DOM from wildfire ash leachates are not well understood. To establish a range of properties, wildfire DOM leachates were generated from (i) surficial [grey and black] wildfire ashes, (ii) mineral soils below ash, and (iii) unimpacted soils from two Colorado wildfire scars. Subsequently, the leachates were studied under simulated sunlight. Photochemical properties of absorbance, fluorescence and $^1O_2$ quantum yield (Φ_F and $\Phi_{^1O_2}$) were determined for thirteen wildfire leachates. $\Phi_{^1O_2}$ of ash leachates was greatest (7.6 ± 3.4%), followed by underlying mineralized soil leachates (4.6 ± 0.7%), and control soil leachates ($\Phi_{^1O_2}$ = 3.9 ± 1%). Correlations between increasing E_2 : E_3, Φ_F, $\Phi_{^1O_2}$ suggest that surface ash leachates with elevated molar absorptivity may play an important role in $^1O_2$ production that is not well documented. Interestingly, photobleaching experiments comparing ash DOM to unimpacted soil DOM revealed ash leachates lost fluorescence, absorbance, while producing CO_2 at rates ~3 fold greater than soils. This suggests that aromatic features of ashes may cause degradation of wildfire DOM faster than unimpacted DOM in the environment.

Received 16th October 2024
Accepted 14th January 2025

DOI: 10.1039/d4em00626g

rsc.li/espi

Environmental significance

Wildfires can significantly affect watersheds. Post-fire rain events can carry large amounts of materials into streams, including wildfire-affected dissolved organic matter (WDOM). This WDOM can then impact the downstream river and communities that rely on the impacted water for their drinking water supply. This study investigates the fate of WDOM in surface waters by examining its photoreactivity, photomineralization to CO_2, and photobleaching of various ash leachates, providing insights into the biogeochemical cycling of wildfire impacted ecosystems. Understanding the distinct photophysical and photochemical properties of WDOM can be used to differentiate it from unimpacted DOM and understand WDOM persistence in the environment.

1 Introduction

The incidence of wildfires in the US and globally is on the rise, driven by factors such as fire suppression at the urban and forested interface and anthropogenic climate change.[1–3] In the Rocky Mountains range of the western US and Canada, the longer and more intense droughts have left forests more prone to bark beetle infestation, tree death, and drier fuels that increase wildfire intensity.[4] Wildfire-prone forests also serve as important watersheds and sources of drinking water. When wildfires and storms occur, heavy fluxes of ash and altered organic matter are introduced to waterways that can severely affect the engineered water treatment systems downstream.[5] Effects such as increased disinfection byproduct (DBP) formation, treatability, or coagulation issues can occur.[6,7] In addition to short-term effects, recovering burn scars alter long-term carbon and nutrients loading and microbial utilization of organic matter in stream ecosystems.[8–12]

After wildfires and rain events release altered dissolved organic matter (DOM), wildfire-derived DOM becomes susceptible to significant solar exposure. Recent work on the optical and molecular properties of wildfire-derived DOM demonstrates that this material has elevated aromaticity, absorptivity, and fluorescence, making it chemically distinct from unburned aquatic DOM.[13–20] Literature indicates that laboratory-generated dissolved black carbon (DBC) have similar optical properties to wildfire-derived DOM and that photoirradiation of DBC induces losses in absorbance properties and a decrease in carbon aromaticity.[21–27] However, the similitudes and differences

[a]*Department of Civil, Environmental and Architectural Engineering, University of Colorado at Boulder, Boulder, 80309, USA. E-mail: Frank.Leresche@Colorado.edu*

[b]*Environmental Engineering Program, University of Colorado Boulder, Colorado 80309, USA*

† Electronic supplementary information (ESI) available. See DOI: https://doi.org/10.1039/d4em00626g

‡ Current address: Department of Civil and Environmental Engineering, University of Missouri, Missouri 65201, USA.

§ Current address: Institute for Biogeochemistry and Pollutant Dynamics, ETH Zurich, Universitaetstrasse 16, 8092 Zurich, Switzerland.

between DBC and ash leachates are not exactly known and the photochemical behavior of wildfire DOM, including reactive intermediates (RI) formation, remains poorly understood. Upon solar irradiation, DOM produces a variety of RIs such as hydroxyl radical ($^{\bullet}OH$), DOM excited triplet states ($^{3}DOM^{*}$) and singlet oxygen ($^{1}O_2$).[28] These short-lived RIs can react with contaminants in surface water, contributing to their degradation, and are also known to react with DOM itself, leading to DOM photobleaching (*i.e.*, loss of absorptivity) and DOM photomineralization.

DOM photobleaching is attributed to both reactions with RIs and to direct sunlight absorption,[29] factors that may affect photobleaching rates include the presence of halogens,[30] and potentially $^{\bullet}OH$, as $^{\bullet}OH$ has been shown to significantly contribute to photobleaching in aerosol particulate matter extracts.[31] DOM isolates photomineralization was recently studied in our group and direct photolysis, $^{3}DOM^{*}$ and $^{1}O_2$ were seen to be significant contributing factors, while $^{\bullet}OH$ was shown to be a relatively minor factor in DOM photomineralization.[32]

Fire can produce both reducing and oxidizing chemical environments.[3] It is known that DOM oxidation (chlorine and ozone treatment) leads to significant increases in $^{1}O_2$ quantum yield ($\Phi_{^1O_2}$).[33,34] Additionally, soot, char and black carbon extracts produced under controlled, anaerobic reducing flame conditions exhibited significant variation in $\Phi_{^1O_2}$, with reported values ranging from 0.21% to 33%.[35–41] These results suggest that wildfire-derived DOM could affect RIs production, yet the exact effects of natural wildfires outside of laboratory settings on soil organic matter $\Phi_{^1O_2}$ are not known. Overall, this study addresses these unknowns by investigating $^{1}O_2$ production in wildfire ash extracts and their photobleaching and photomineralization under simulated sunlight irradiation. Following a wildfire event, surficial grey ashes, mineral soils beneath the ash layer, and unimpacted soils were collected and studied for their optical properties *via* excitation emission matrices (EEMs), absorbance spectra, and *via* a novel size-exclusion chromatography system (SEC-Φ_F).[42] These analyses highlight how optical properties and SEC-Φ_F for different natural wildfire materials change during photoirradiation experiments. Changes in CO_2 production and oxygen consumption to CO_2 formation ratio ($O_2 : CO_2$) was also monitored during the photoirradiation experiments to assess mineralization across various wildfire DOM. Lastly, a kinetic analysis was performed using $^{1}O_2$ as proxy for both $^{1}O_2$ and $^{3}DOM^{*}$ effects. The analysis linked $^{1}O_2$ to the photobleaching rate, delineating the relative importance of indirect photochemistry in the photobleaching process.

2 Experimental

2.1 Sampling locations and sample descriptions

Ashes and burned mineral soils were collected in 2018, 2019, and 2020 from two burn scars in the Rocky Mountains, Colorado and Wyoming/Colorado, USA (Fig. S1†). The burn scars were caused by the 2018 Ryan Fire, which impacted ~88 km^2 of forest, and the 2020 Cameron Peak Fire that impacted ~884 km^2 of forest. The subalpine forests consisted of predominately lodgepole pine (*Pinus contorta*) and mixes of Engelmann spruce (*Picea engelmannii*) and subalpine fir (*Abies lasiocarpa*). Additional details of burn scars and soils/ash are further described in Fischer *et al.*[20] Ashes from the Ryan fire were collected in 2018 within 1 month of the fire containment and before development of the winter snowpack. Mineral soils from the Ryan Fire were collected 1 year later in September 2019 on exposed weathered soils. Ashes from the Cameron Peak Fire were collected in November 2020 prior to any significant precipitation on the burn scar. Burned mineral soils were collected from the soil top layer (0–10 cm depth) after withdrawal of the overlaying ash and char material, while ashes were collected directly from the top layer. pH, leachable DOC and elemental analysis of the extracts are presented in Fisher *et al.*[20] pH was measured to be lower for the unburned soils (pH = 6.1 ± 0.9) than the burned mineral soils (pH = 6.5 ± 1.1) and the ashes (pH = 8.2 ± 0.6), while the leachable DOC followed an opposite trend, with higher values for the control soils than the burned mineral soils and lower values for the ashes. Leachates were not characterized for ionic content. Wildfires are known to influence the release of photoactive materials; *e.g.*, an increase in nitrate and a decrease in iron concentration were reported by Sanchez *et al.*[10] Ashes may also contain other cations such as Ca, Si, Mg, and K, reflective of soils and plant species burned, and inorganic carbonates and oxides.[43] These constituents may have contributed and influenced hydroxyl radical formation that was not the main focus of this paper.

All ash and soils were collected with trowels into polypropylene gallon bags and transported in dark coolers. Materials were sieved with a 2 mm sieve, completely dried in a 45 °C oven for several days and stored long term in combusted glass jars. For this study, all samples were categorized as (i) unburned soils collected adjacent to burn scars, (ii) burned mineral soil collected below or after weathering of an ash and loose debris layer, and (iii) ash layer samples collected from surface burn scar surfaces, typically grey or black in color (Table S1†). The thirteen samples in this study were a subset from the data presented in Fischer *et al.*[20] that presented absorbance and fluorescence characteristics of forty leachates. The subset samples herein were selected to represent three main types of unburned, mineral burned soils, and ash samples from both burn scars and were studied for $\Phi_{^1O_2}$ experiments herein (Table S1†). Two grey surface ashes and one unburned soil were used for further photoirradiation experiments and size exclusion chromatography (SEC-Φ_F) characterization.

2.2 Chemicals and solutions

All chemicals were used as received except for *p*-nitroanisole (PNA) that was recrystallized in ethanol. All solutions were prepared using ultrapure water (resistivity ≥ 18.2 MΩ cm) obtained from a Sartorios Stedim dispenser or equivalent. Pyridine, CAS N_0: 110-86-1, Mallinckrodt chemicals, purity min. 99%. *p*-Nitroanisole, 100-17-4, recrystallized. Calcium chloride dihydrate, 10035-04-8, VWR, 99%+ Trace Metal Grade ACS Reagent. Furfuryl alcohol, 98-00-0, TCI, 97%. Phosphoric acid, 7664-38-2, EMD Millipore, 85% w/w in H_2O. Sodium phosphate dibasic anhydrous, Sigma-Aldrich, 7558-79-4 (≥99%), sodium

phosphate monobasic monohydrate, Sigma-Aldrich, 10049-21-5 (≥99.5%), sodium sulfate, Sigma-Aldrich, 7757-82-6 (≥99%), ammonium acetate, Sigma-Aldrich, 631-61-8 (≥98%), ammonium bicarbonate, Sigma-Aldrich, 1066-33-7 (99–101%), hydrochloric acid, Sigma-Aldrich, 7647-01-0 (37%), acetonitrile, VWR, HPLC grade. Methanol, VWR, HPLC grade.

2.3 Analytical instrumentation

Dissolved organic carbon (DOC) was measured on a Sievers TOC analyzer model M5310C. Fluorescence spectra were measured at room temperature using a Horiba Scientific FluoroMax-4 spectrofluorometer and 1 cm quartz cuvette. Absorbance spectra were measured at room temperature using a Cary 4000 UV-vis or a Cary 100 Bio UV-Visible spectrophotometer (Agilent Technologies) and 1 or 5 cm pathlengths quartz cuvettes. Concentration of the probe compounds was measured on an Agilent 1200 high-pressure liquid chromatography (HPLC) system equipped with an Agilent Eclipse C-18 5 μm particle size reversed phase column using the methods described below. Photoreactor and solar simulator emission spectra were measured using an Ocean Optics USB2000 spectrophotometer.

For furfuryl alcohol detection, the eluent used was 65% 10 mM phosphoric acid and 35% methanol at 1 mL min^{-1}, with a retention time of 2.9 min, and detection wavelength of 219 nm. For *p*-nitroanisole, the eluent used was 50% 10 mM phosphoric acid and 50% acetonitrile at 2 mL min^{-1}, with a retention time 2.3 minutes, and detection wavelength of 300 nm.

Dissolved oxygen was quantified using a Firesting O_2 Fiber-Optic Oxygen Meter and high-speed needle-type, oxygen sensor (OXR50-HS). CO_2 formation was measured using Agilent 7890A gas-chromatography with a 100-psi split/spitless inlet and an Agilent 7693A automatic sampler. The system was configured with a 0.53 mm diameter Agilent HP-Plot-Q column, a Nickel Catalyst accessory to convert carbon products to methane, and an Agilent flame ion detection (FID) system (see Table S2† for additional information).

An Agilent 1260 high-pressure liquid chromatography system (HP-SEC), coupled with a Toyopearl HW-50S size exclusion chromatography column (SEC), was used to assess the apparent molecular weight (AMW) distribution of samples before and after solar exposure. 1.8 mL of each sample was injected using a 1260 Infinity II Agilent Vialsampler. Phosphate buffer mobile phase consisted of 0.0016 M Na_2HPO_4, 0.0024 M NaH_2PO_4, and 0.0031 M Na_2SO_4, with an ionic strength of 0.1 M, resulting in a final pH of 6.8 and conductivity of 6.8 mS cm^{-1} and flowed at 1 mL min^{-1} through a 1260 Infinity Diode Array and Multiple Wavelength Detector (DAD) scanning at 200–700 nm in 2 nm increments, followed by an Agilent 1260 Infinity Fluorescence Detector (FLD) at $\lambda_{ex} = 300$ nm, $\lambda_{em} = 300$–700 nm in 5 nm increments. In-line total organic carbon (TOC) measurements were taken using an in-line Sievers M9 Total Organic Carbon Analyzer.

2.4 Leaching of ashes

To generate fresh wildfire DOM for experiments herein, four grams of dry soil or ash were combined with 40 mL of fresh 0.01 M $CaCl_2$ leaching solution in 50 mL centrifuge tubes. The 0.01 M $CaCl_2$ solution was chosen to model natural water ionic strength with low optical interference following Gabor *et al.*[44] Samples were agitated for 16 hours and gently centrifuged prior to filtering. The leachate supernatant was filtered through a pre-rinsed 0.45 μM glass fiber filters (Whatman GD/X) and the resulting solutions were stored in combusted amber glass vials. Leaching solutions and filtered leachates were stored in combusted amber glass at 4 °C for up to one month.

2.5 $^1O_2$ measurements

The methods to measure and calculate the production and quantum yields of $^1O_2$ produced under irradiation are described in detail elsewhere[45] and in Text S1,† but briefly: $^1O_2$ was measured by spiking the solutions with 22.5 μM furfuryl alcohol (FFA) as a probe compound in the presence of 0.1 M methanol as a hydroxyl radical quencher. Control experiments indicated that FFA direct photolysis is negligible during an experiment (Fig. S2†). The solutions were irradiated using a RPR100 Rayonet merry-go-round photoreactor equipped with 16 RPR-3500A light bulbs that had an emission spectrum centered around 366 nm (Fig. S3†). 100 μL solution aliquots were taken at regular time intervals and FFA analyzed using the aforementioned HPLC system. The FFA concentration was fitted using a pseudo-first order kinetic model using the software Origin 2020. $^1O_2$ steady-state concentration ($[^1O_2]_{ss}$) was determined using $k_{^1O_2,FFA}$, the second-order rate constant between $^1O_2$ and FFA of 1.00×10^8 M^{-1} s^{-1}.[46] $\Phi_{^1O_2}$ was then determined as $^1O_2$ production rate divided by the rate of light absorption. It should be noted that at the laboratories elevation (1655 m), the atmospheric pressure is ≈82 000 Pa and the corresponding $[O_2]$ value for 22 °C air-saturated solution of ≈230 μM. Compared to lower-level elevations, the lower $[O_2]$ value induces lower $[^1O_2]_{ss}$ and $\Phi_{^1O_2}$. The Rayonet merry-go-round photoreactor was chosen over the solar simulator (used in the photoaging experiments) for its better accuracy in $[^1O_2]_{ss}$ and $\Phi_{^1O_2}$ measurements. The main source of measurement error was the wildfire DOM absorbance. The shorter wavelength range of the Rayonet irradiation excluded longer visible wavelengths from the calculations, where wildfire DOM exhibits low absorbance.[47]

The photon fluence was measured daily using the PNA–pyridine actinometry. This actinometry is detailed elsewhere,[45] but briefly solution of 10 μM PNA and 5 mM pyridine were irradiated and 100 μL solution aliquots taken at regular time intervals and PNA concentration analyzed similarly as FFA. The photon fluence in the 340–410 nm interval was calculated to be 1.4×10^{-3} mol m^{-2} s^{-1}.

2.6 Photoaging irradiation experiments

Ash leachates were irradiated with an Oriel Sol1A solar simulator, using a 1000 W xenon lamp (operated at 800 W) (Fig. S3†). The extracts were irradiated for intervals of $t = 0$, 4, 6, 8, 16 or 24

hours in 5 mL clear glass vials. Vials were positioned at an angle of ≈30° from the horizontal in a temperature-controlled water bath ($T = 20 \pm 1$ °C). The photon fluence was evaluated similarly as for the Rayonet photoreactor using the PNA–pyridine actinometry. Fluence was calculated to be of 4.3×10^{-4} mol m^{-2} s^{-1} in the 290–400 nm interval. For comparison, the noon clear sky 290–400 nm photon fluence for Boulder, Colorado was calculated to be 3.07×10^{-4} mol m^{-2} s^{-1} for the summer solstice, 2.61×10^{-4} mol m^{-2} s^{-1} for the equinoxes and 1.63×10^{-4} mol m^{-2} s^{-1} for the winter solstice.[31] Oxygen concentration was measured using the aforementioned oxygen probe and seen to decrease during the 24 hours experiments from ≈8 to ≈4 mgO_2 L^{-1} (Fig. S4†).

2.7 CO_2 measurements

CO_2 production was measured at the end of the photobleaching experiments in separate experiments. For the leached DOM samples to be compatible gas chromatography and size exclusion chromatography, the $CaCl_2$ used to leach samples was removed using the solid phase extraction (SPE) protocol outlined in Dittmar *et al.*[48] Each leachate was acidified to pH = 2 using 1 M hydrochloric acid (HCl) and extracted using 200 mg Agilent Bond Elut cartridges. This method is known to retain a proportional distribution of fractions of DOM and had a 70–94% DOC recovery for leachates in this study. Cartridges were dried under N_2 gas for >5 minutes, extracted using 6 mL of methanol, evaporated to dryness using a TurboVap LV evaporator, and reconstituted in 6 mL of water. TOC was checked using the aforementioned TOC analyzer. The UV spectra of samples before and after SPE showed little to no variation, further suggesting high recovery (Fig. S5†). Each sample was diluted to 10 mg$_C$ L^{-1}, buffered with 10 mM ammonium acetate, adjusted to pH 6 using HCl, and capped without headspace in a 2 mL GC borosilicate glass crimp vial. Samples were irradiated for 24 hours at a temperature of 20 °C using the solar simulator at operational parameters as described in Section 2.6. Each experiment was performed in duplicate.

Immediately following irradiation, 0.5 μL volume of each sample was injected in at least duplicate into GC-FID and paired methanizer to measure CO_2 concentration. Ammonium bicarbonate and HCl were combined to form CO_2 in known concentrations which were used to generate a standard curve for CO_2 formation as shown in eqn (S6) and Fig. S6.† A Suwannee River fulvic acid standard was also run to verify consistency.

2.8 Size exclusion chromatography measurements

To assess the apparent molecular weight (AMW) distribution of samples before and after solar exposure, each sample was run on HP-SEC. Each leachate was diluted to 5 mg$_C$ L^{-1} in 10 mM phosphate buffer and solar simulated for 24 hours in at least duplicate. Samples were spiked with concentrated mobile phase to adjust the sample conductivity and pH to that of the mobile phase. Absorbance, fluorescence, and DOC chromatograms were processed and corrected to calculate a continuous Φ_F chromatogram as a function of AMW as shown in other studies.[42,49] Refer to Hanson *et al.*[42] for the detailed Φ_F calculations. Φ_F was not calculated when absorbance intensities were below 0.5 mAu, as weak signal results in unreliable Φ_F values.

2.9 Optical parameters

Optical parameters were calculated from the UV-Vis absorbance and fluorescence data. The $E_2:E_3$ ratio is the ratio of the absorbance value at the wavelength $\lambda = 250$ over the absorbance at 365 nm. The specific ultraviolet absorbance (SUVA$_\lambda$, unit L mg$_C^{-1}$ m^{-1}) is the absorbance at the wavelength λ over the carbon concentration. Φ_F was calculated for the excitation wavelength of 350 nm similarly as in Leresche *et al.*[34]

3 Results and discussion

3.1 Fluorescence and singlet oxygen quantum yields

Φ_F of control unburned soil leachates were in the 0.8–2.2% range, while mineral soil leachates and ash leachates exhibited Φ_F in the 1.3–4.2% and 3.4–5.3% range, respectively (Fig. S7†). Soil humic isolates typically exhibit a Φ_F of 0.4–1.1%,[50] which is in the lower range of values measured in this study, indicating that fire exposure contributes to an important increase in Φ_F. This is further supported by laboratory observations that indicated that heat-treated soils have increased Φ_F.[14] $\Phi_{^1O_2}$ of the control unburned soil leachates was measured in the 2.6–4.9% range, while mineral soil leachates were in the 3.0–5.3% range, and ash leachates were in the 2.4–13% range. Soil organic matter data from the Ossola *et al.* review[47] have mean $\Phi_{^1O_2}$ values of 1.4% and a range of values of 0.4–5.4%. $\Phi_{^1O_2}$ values for the control soil leachates fell into that expected range. Mineral soil leachates had higher values, while the ash leachates were significantly higher values (up to 13.5%), indicating that the fire exposure induced an important $\Phi_{^1O_2}$ increase in the ash extracts.

With the high variability of fire conditions (temperature, oxygen), it is expected that both local reducing and oxidizing environments exist during a wildfire. The ash topsoil is expected to undergo more oxidizing conditions compared to the underlying mineral soils where oxygen-poor reductive conditions become more prevalent. Soot and dissolved black carbon extracts that are produced under reducing flame conditions exhibited variable $\Phi_{^1O_2}$ values depending on the study, with $\Phi_{^1O_2}$ of 33% for a soot extract,[35] and 3.4–6.6%,[36] 0.55–0.81%,[38] and 4.1%[37] for dissolved black carbon. Two recent papers investigating the factors that lead to this $\Phi_{^1O_2}$ variability indicated that the source material and the pyrolysis temperature were both influencing $\Phi_{^1O_2}$,[39] and that for lab generated dissolved black carbon, a higher pyrolysis temperature (200–500 °C) leads to higher $\Phi_{^1O_2}$ values (0.21–1.77%), which the authors attributed to the formation of quinones.[41] When considering oxidative conditions, studies have shown that DOM treated with chlorine or ozone (both oxidants) exhibited important increase in $\Phi_{^1O_2}$ values up to 8.4% and 17.1% respectively.[33,34] For ozone, this increase was attributed to the oxidation of phenols to quinones, which are known to have high $\Phi_{^1O_2}$ values.[34] Phenols O–H bond

being relatively reactive, with homolytic bond dissociation energy (BDE) of 377 for phenol and 330–371 kJ mol^{-1} for methoxy-substituted phenols, as a comparison, the C–H BDE in benzene and ethane are 472 and 423 kJ mol^{-1} respectively, and the O–H bond in ethanol of 438 kJ mol^{-1}.[51,52] This indicates that both reducing and oxidizing flame conditions can potentially lead to an increase in $\Phi_{^1O_2}$ and that the observed $\Phi_{^1O_2}$ increase can likely be attributed to the profound DOM transformations induced by the fire, and tentatively to the formation of quinones from the oxidation of phenols.

Wildfires are known to increase the aromatic C fraction in the soil and to produce black carbon-like compounds that are mostly aromatic.[53] The observed increase in Φ_F can likely be attributed to cyclization and condensation reactions, forming a range of aromatic compounds that have high Φ_F (*e.g.*, benzene $\Phi_F = 4\%$,[54] naphthalene $\Phi_F = 21\%$,[55] phenanthrene $\Phi_F = 13\%$,[55] note that these values were measured in ethanol and that the solvent can affect Φ_F).

3.2 Optical parameters correlation

Optical parameters, such as the $E_2:E_3$ ratio or SUVA, that correlate with DOM molecular size, aromaticity and photoreactivity,[56,57] are often used to characterize DOM. Fig. 1A presents relationships between $\Phi_{^1O_2}$ and $E_2:E_3$. A linear relationship can be observed between $\Phi_{^1O_2}$ and $E_2:E_3$ with a slope of 0.021 for the ashes and 0.0065 for the underlying mineral soils. The regression did not yield well correlated results for the control unburned soils. For comparison, the same regression slope parameter for Everglade DOMs was 0.0064,[58] various aquatic origin DOMs was 0.0087,[59] fractionated DOM isolates ranged between 0.01–0.017,[57] ozonated DOM ranged between 0.0039–0.011,[45] and chlorinated DOM ranged from 0.037–0.094.[33] Fig. 1B presents $\Phi_{^1O_2}$ *vs.* Φ_F. It can be observed that there is a correlation between the two quantum yields. This correlation was also observed for ozone treated DOM and was postulated to come from a decrease in the internal conversion rate that would subsequently increase both $\Phi_{^1O_2}$ and Φ_F, as internal conversion competes with both fluorescence and singlet oxygen production.[34,60] Fig. S8† presents $\Phi_{^1O_2}$ *versus* $SUVA_{254}$. The observed correlations for $SUVA_{254}$ have lower Pearson correlation coefficients compared to the $E_2:E_3$ ratio. McKay *et al.*[14] presented a linear relationship between the heating temperature and $SUVA_{254}$ for thermally heated soils. The range of $SUVA_{254}$ observed here (1.3–4) for the ashes extract can be compared to this regression line and would fall in the $SUVA_{254}$ values observed for soils heated in the 150 to 250 °C range. This can be rationalized by considering that temperatures higher than 200–250 °C induce significant mass loss for hemicellulose and cellulose,[61] and that for thermally heated soils the extractable carbon fraction decreases with increasing temperature exposures, *e.g.*, by a factor 10 between 150 and 250 °C.[14]

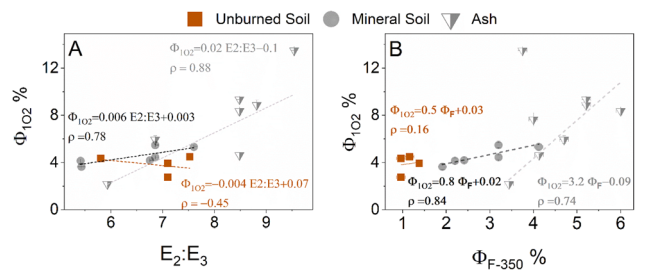

Fig. 1 Relationships between $E_2:E_3$, singlet oxygen and fluorescence quantum yields ($\Phi_{^1O_2}$ and Φ_F respectively). Brown squares: control unburned soils, dark grey circles: mineral soils and light grey split triangles: wildfire ashes. $E_2:E_3$ is the ratio of the absorbance at 250 nm over the absorbance at 365 nm. The Pearson correlation coefficients (ρ) of the linear regressions are presented for each sample type. Note that the slope and intercept values presented refer to the absolute $\Phi_{^1O_2}$ values.

The observed relationship between the $E_2:E_3$ ratio (that inversely correlate with molecular weight and aromaticity) and $\Phi_{^1O_2}$ indicates that ash extracts, which have lower molecular weight and lower aromaticity, also have the higher $\Phi_{^1O_2}$. It can be postulated that the ash extracts with higher $\Phi_{^1O_2}$ were the most impacted by the fire. The correlation between $\Phi_{^1O_2}$ and Φ_F probably indicates that wildfire induces changes in the soil DOM composition that results in a decrease in the internal conversion rate, as was postulated for ozone treated DOM.[34]

3.3 Effects of photoirradiation on leachates

3.3.1 Change in absorbance and mineralization to CO_2. Simulated sunlight irradiation experiments were conducted on two fire-exposed ash leachates and one control unburned soil leachate. The two wildfire leachates absorb more light (2.8 and 3.5 times for Black Hollow Creek (BHC) and Seven Mile Creek (SMC) respectively in the interval 250–450 nm) than the control soil leachate. Irradiation induces a decrease in absorbance (photobleaching) and in Φ_F, the relative decrease in absorbance at longer wavelengths being more pronounced (Fig. 2A, 4 and S9–S11). CO_2 was measured at the end of the 24 h irradiation and the percentage of mineralized carbon was calculated to be 10–12% for the burned extracts and 4% for the control soil extract (Fig. 2B). The $O_2:CO_2$ ratio (consumed O_2 over produced CO_2) was calculated to be 2.3 for the control soil and of 0.9–1.1 for the burned ash extracts (Fig. 2C). SEC results presented in Fig. 3 as high, medium and low molecular weight fractions (see Fig. S12† for the full chromatograms and the corresponding fractions) indicate that the control soil leachate had a higher overall apparent molecular weight compared to the ash leachates. Irradiation induced a shift to lower molecular weight for the control soil leachate, and a decrease in absorbance, fluorescence and Φ_F for all three leachates (Fig. 3 and S12†).

The observed photobleaching concords with literature observations of DOM absorbance loss upon photoirradiation.[29,62–64] The general trend observed in the literature for terrestrial and aquatic derived DOM is that photoirradiation induces a loss in DOC and a decrease in molecular weight, and that DOM composition changes to less aromatic and more aliphatic distributions of carbon.[65,66] The results presented in Fig. 2 and 3 concord well with the DOM literature, indicating that photoirradiation induces similar effects on ash leachates and DOM.

The increased CO_2 formation and decreased $O_2:CO_2$ in ash leachates compared to the control soil suggests that wildfire

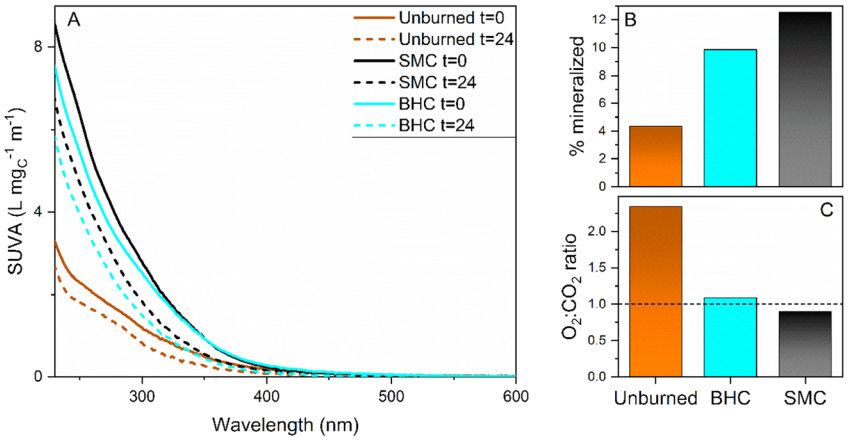

Fig. 2 Change of absorbance spectra, CO_2 production and O_2 : CO_2 ratio for three ash leachates under simulated sunlight irradiation. (A) Specific UV-Vis absorbance (SUVA) for non-irradiated samples ($t = 0$) and after 24 hours of irradiation. (B) percent of carbon that was mineralized to CO_2 upon 24 hours of simulated sunlight irradiation. (C) O_2 (consumption):CO_2 (production) ratio upon 24 hours of irradiation. Brown, control unburned site extract. Cyan, Black Hollow Creek (BHC) extract. Black, Seven Mile Creek (SMC) extract.

induces compositional changes such as the formation of readily-mineralizable compounds classes. The $O_2 : CO_2$ ratio can be interpreted by considering that O_2 is the electron acceptor, and that the oxygen consumption depends on the change in carbon oxidation state. For example, methane combustion (carbon-IV) uses 2 molecules of O_2 for 1 produced CO_2 ($O_2 : CO_2$ ratio = 2) while the combustion of coal (carbon 0) uses 1 molecule of O_2 for 1 produced CO_2 ($O_2 : CO_2$ ratio = 1). Note that reactions that do not produce any CO_2 can consume oxygen, this can be expected from $^1O_2$ if it participates in Diels–Alder like reaction or from $^{\bullet}OH$ that can participate in addition reaction (*e.g.*, the conversion of benzene to phenol). This analysis indicates that the aforementioned ash leachates readily mineralizable compounds classes, have carbon with high oxidation state. A potential example of such class could be the benzene and pyridine polycarboxylic acids recently detected in wildfire ashes extracts that could undergo decarboxylation under photoirradiation,[67–70] such carboxylic acids were postulated to be a major factor in the CO_2 production from permafrost dissolved organic matter photoirradiation,[71] and were seen to be more sensitive that the rest of the DOM pool to photoirradiation.[72] Literature indicates that benzene carboxylic acids are sensitive to both direct photodecarboxylation reactions and indirect photodecarboxylation with $^1O_2$ or triplet photosensitizers such as aromatic ketones and quinones.[73,74] Recent results on the factors that influence DOM photomineralization to CO_2 indicate that direct photolysis, $^1O_2$ and ^{3}DOM* are major factors.[32] Since $[^3DOM^*]_{ss} \approx [^1O_2]_{ss}$,[28] and results above showed that wildfire enhanced $^1O_2$ formation, then it can be postulated that the enhanced formation of $^1O_2$ and ^{3}DOM* may be responsible, to some extent, for increased CO_2 formation. Results of Fig. S12† highlight that after exposure to simulated sunlight, the decreases in Φ_F for the ash leachates was more pronounced in the low molecule weight regions (high elution volumes) compared to the soil control. This suggests that wildfires may induce an increase in low molecular weight fluorophores that are especially sensitive to phototransformation.

3.3.2 Photobleaching kinetics. Del Vecchio and Blough's work on one riverine and two estuary DOM indicated that the decrease in absorbance could be well fitted by a two-part exponential decay.[63] The first of which fit the significant decrease observed within the first 20 h of irradiation, while the second exponential was needed to fit the decrease between 20–200 h. Bostick *et al.* used a similar two-part exponential model to fit the decay in DBC (measured as polycarboxylic acids) over 32 days.[22] Holt *et al.* used a single exponential model that well fitted the absorbance decrease for six DOM of various sources over a 28 day irradiation experiment.[65] Here, we used a single exponential decay function to fit the exponential-like decrease in $SUVA_{254\ to\ 350}$ and Φ_F of two ash extracts (Fig. 4 and S9–S11†). An increase in the $E_2 : E_3$ ratio was also observed (Fig. S13†). The difference in irradiation time between this study and the previous studies from Del Vecchio and Blough and Bostick *et al.* is probably the reason a single exponential function could be used here.

SUVA decrease was fitted by a first-order kinetic decay (eqn (1)), where R is a constant (unit L mg$_C^{-1}$ m^{-1}), S is a pre-exponential factor (L mg$_C^{-1}$ m^{-1}), k is a first-order constant (h^{-1}), and t is the time (h).

$$SUVA_\lambda = R + S\,e^{-kt} \quad (1)$$

The constant R was necessary to obtain a good fit and corresponds to the fraction of the absorbance that is refractory (on the experiments timescale) to photobleaching, while the constant S correspond to the fraction sensitive to photobleaching (note, $SUVA_{t=0} = R + S$). BHC data presented an outlier at time $t = 16$ h and the fittings were repeated without this data point (Fig. S11†). Table S3† presents the obtained fitting parameter with and without this outlier, but in the remainder of the discussion we will discuss only the parameters obtained without the outlier. The obtained first-order constants

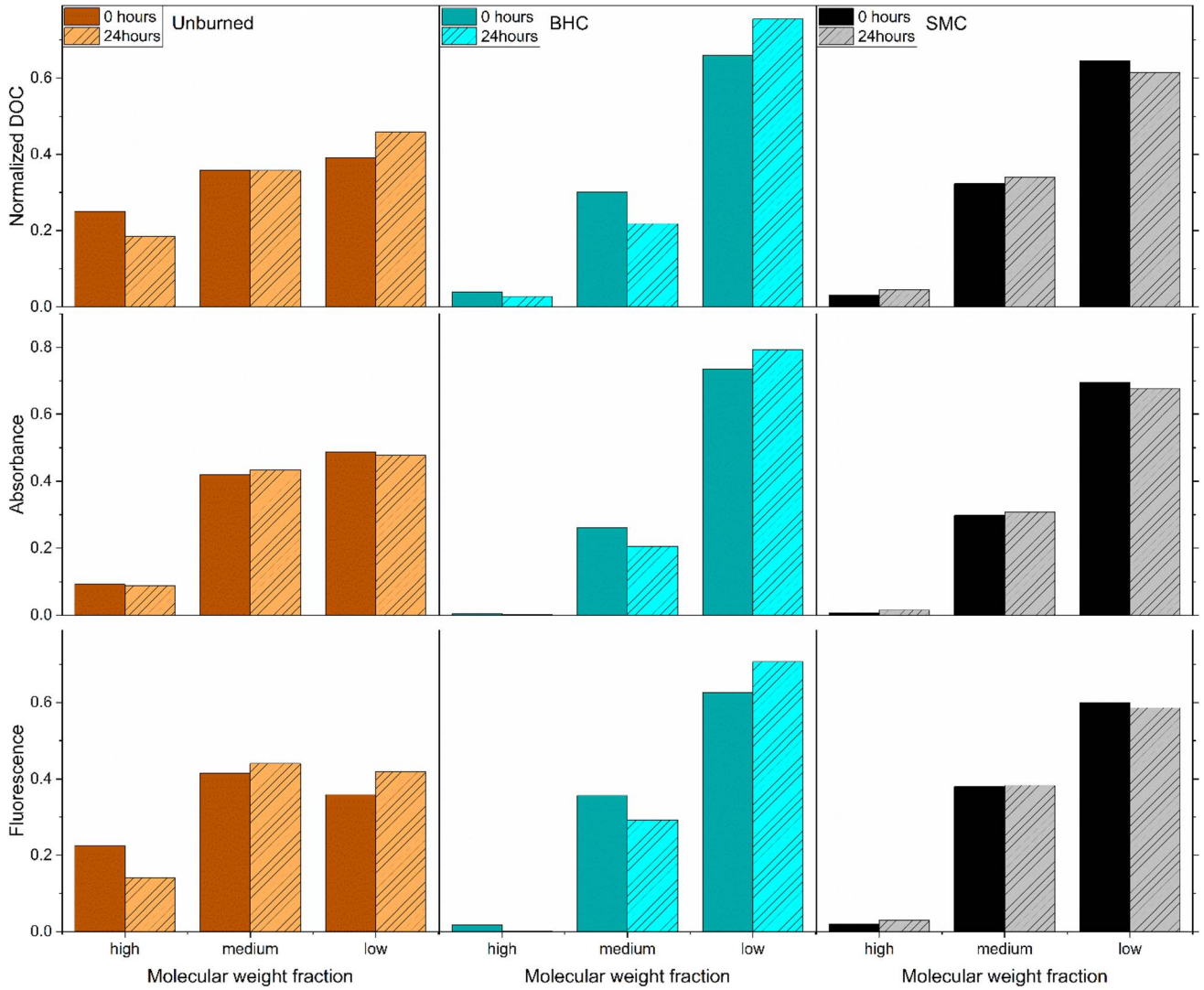

Fig. 3 Size-exclusion relative fractions for three ash leachates before (plain) and after (dashed) 24 hours of simulated sunlight irradiation. Left column (brown), control unburned soil leachate, middle column (cyan) Black Hollow Creek (BHC) ash leachate and right column (black/grey) Seven Mile Creek (SMC) leachate. The fractions were calculated on the elution volume as high molecular weight (30–40 mL), medium molecular weight (40–45 mL) and low molecular weight (45–55 mL) following the methodology presented in Buckley *et al.*[49] For a given SEC chromatogram, the area was integrated for the corresponding fraction and the relative fraction calculated as the ratio of the integrated area over the 30–55 mL area.

k varies for Seven Mile Creek ash (SMC) between 0.07–0.15 h^{-1}, and $\approx$ 0.22 h^{-1} for Black Hollow ash (BHC). The control unburned soil had first-order constants between 0.14–0.23 h^{-1} (Table S3†). It can be observed that the longer wavelengths tended to be more sensitive to photobleaching exhibiting higher first-order constants k. From the fitting, the fraction of the absorbance sensitive to photobleaching, f_s, can be calculated as $f_s = S/SUVA_{t=0}$ where $SUVA_{t=0}$ is the SUVA of unirradiated samples. Values for f_s vary from 19.8–39.7% for SMC extracts and 28.5–52.9% for BHC extracts while the unburned control had lower values of 4.8–32.6% for f_s. It can be observed that f_s is wavelength dependent, with higher values at longer wavelengths indicating that the longer wavelengths are more sensitive to photobleaching. Note that upon photobleaching, chromophores absorbing at 350 nm could produce new chromophores absorbing at shorter wavelengths and that the observed trends could be reflecting this possibility.

The corresponding half-lives ($t_{1/2} = \ln 2/k$) for the obtained k constants at 350 nm are 4.6 $\pm$ 0.9 and 3.5 $\pm$ 0.1 hours for SMC and BHC respectively, indicating that a fraction of the ash extracts is sensitive to photobleaching under environmental conditions. It should be noted that the extracts are composed of various molecules that have variable sensitivity to photobleaching, and the fitted constant represents an average of the individual components' photobleaching constants. For comparison, the half-lives obtained by Bostick *et al.* on DBC disappearance (faster exponential of the two-exponential model) were between 14–24 hours.[22] The increase in $E_2:E_3$ ratio (Fig. S13†) is consistent with literature data that also observed an increase in $E_2:E_3$ upon DOM photoirradiation.[75] As

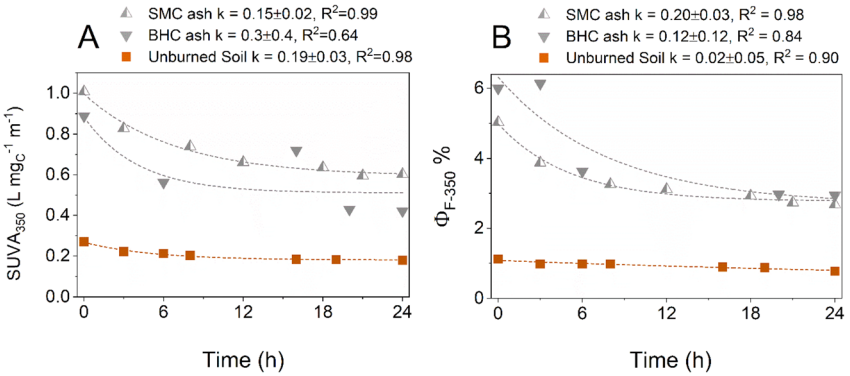

Fig. 4 Decrease in (A) specific ultraviolet absorbance at the wavelength $\lambda = 350$ nm ($SUVA_{350}$) and (B) fluorescence quantum yield (Φ_F) of ashes aqueous extracts as a function of irradiation time (simulated sunlight). Dotted lines represent non-linear fitting curves to an exponential function $y = y_0 + A\,e^{-kt}$. Brown squares: unburned soil leachate, upward split grey triangles Seven Mile Creek wildfire ash leachate (SMC ash), and downward grey triangles Black Hollow wildfire ash leachate (BHC ash). Fig. S9 and S10† present $SUVA_{254}$ and $SUVA_{280}$ data.

$E_2:E_3$ is the ratio of the absorbance at 250 over 365 nm, the increase in $E_2:E_3$ reflects the faster decrease in absorbance at 365 nm than 250 nm.

3.3.3 Indirect photochemistry role. Our recent study on DOM photomineralization revealed that direct photolysis, ^{3}DOM* and $^1O_2$ were seen to be significant contributing factors, while $^{\bullet}$OH was seen to be a relatively minor factor in photomineralization of DOM isolates.[32] The objective of this section was to perform a kinetic analysis investigating the role of ^{3}DOM* and $^1O_2$ indirect photochemistry in DOM photobleaching. Given that ^{3}DOM* is a mixtures of compounds with different reactivities, it is challenging to measure $[^3DOM^*]_{ss}$, and the reactivity of each individual ^{3}DOM* species is not well defined.[76] This is not the case for $^1O_2$ which can be measured more easily, and the published rate constants towards many classes of compounds are more readily available.[77] In surface waters $[^3DOM^*]_{ss} \approx [^1O_2]_{ss}$, and ^{3}DOM* is relatively more reactive than $^1O_2$ for many compound classes.[76,78,79] This indicates that the kinetic analysis for $^1O_2$ presented here can also be qualitatively applied to ^{3}DOM*.

$^1O_2$ reactions can result in the incorporation of oxygen atoms in the resulting product,[80] and several studies have indicated that $^1O_2$ can react with specific DOM components.[64,81] For Suwannee River and Pony Lake fulvic acids, Cory *et al.* attributed 64–70% of the oxygen uptake to $^1O_2$ reactions (indicating that other mechanisms also played a role).[82] The observation that aging of wildfire impacted DOM leads to an increase in the O/C ratio, may indicate that $^1O_2$ is involved in the aging process.[19] By measuring $^1O_2$ steady-state concentration ($[^1O_2]_{ss}$) during the ash photobleaching experiments, it is possible to calculate the half-lives of compounds with known $^1O_2$ second-order rate constants ($k_{^1O_2,P}$) in these $[^1O_2]_{ss}$ conditions and compare the calculated half-lives to the absorbance half-life determined in the exponential fitting above. The pseudo-first order constants of various compounds are calculated as the product of $[^1O_2]_{ss}$ and $k_{^1O_2,P}$. Their corresponding half-life is calculated as the ratio of ln(2) over the calculated pseudo-first order constant. Table 1 presents the theoretical half-life of a variety of compounds due to $^1O_2$ in the two ashes extracts under simulated sunlight. The compounds were selected from the Wilkinson *et al.* review,[77] and are representative of structures that either may be present in DOM or similar to compounds recently detected in wildfire ash extracts (carboxylic acid substituted pyridines and quinolines compounds).[67–69] Note that some of the literature second-order rate constants $k_{^1O_2,P}$ were measured as $^1O_2$ deactivation (k_d), while others were measured as the disappearance of P (k_r), and that k_d can be higher than k_r, and the use of k_d may lead so to an shorter estimate of a compound half-life.

It should be noted that reactions with $^1O_2$ are not the only phototransformation process occurring under sunlight irradiation, as direct photolysis and others photochemically produced reactive species such as ^{3}DOM* or $^{\bullet}$OH may also contribute to the phototransformation of compounds in surface waters. It should also be noted that the $^1O_2$ measured is the bulk $^1O_2$ and that $^1O_2$ concentration in the DOM microdomain is higher than the bulk one.[84,85] This also applies to other RIs such as ^{3}DOM* an $^{\bullet}$OH.[86,87] The higher RIs concentration in the DOM microdomain would lead to the real lifetime being shorter. Table 1 indicates that the location of a substituent can influence the reactivity (*e.g.*, $k_{^1O_2,P}$ of dihydroxy substituted naphthalene varies between 6.8×10^5 to 3.0×10^7 M^{-1} s^{-1}). Table 1 also indicates that to correspond to the measured $SUVA_{350}$ half-lives of ≈4 hours (see above), compounds should have a $k_{^1O_2,P}$ of $\approx 7.0 \times 10^7$ M^{-1} s^{-1}. For the pyridines and quinolines, which are classes of compounds recently detected is wildfire ashes,[67,68] Table 1 indicates that the reactivity of quinolines compounds towards $^1O_2$ is sufficient to explain the observed $SUVA_{350}$ attenuation (≈4 hours). While for the pyridines, their reactivities towards $^1O_2$ are too low to explain the observed $SUVA_{350}$ attenuation. As $[^3DOM^*]_{ss} \approx [^1O_2]_{ss}$,[28] and since anilines have high reactivity towards models ^{3}DOM* sensitizers (1×10^7 to 5×10^9 M^{-1} s^{-1}),[88,89] it can be hypothesized that pyridines also have high reactivity towards ^{3}DOM* and that the reactivity of pyridines towards ^{3}DOM* could lead to their disappearance in the observed timeframe. This kinetic analysis concurs with

Table 1 Calculated singlet oxygen ($^1O_2$) half-life for a series of selected compounds in Seven Mile Creek ash (SMC) or Black Hollow ash (BHC) aqueous extract

Compound	$^1O_2$ second-order rate constant[a] ($k_{^1O_2,P}$, M^{-1} s^{-1})	Solvent[b]	k_d or k_r[c]	Half-life Seven Mile Creek ash[d] (h)	Half-life Black Hollow ash[d] (h)
Phenol	1.0×10^6	H_2O pH 8	k_r	289	216
Naphthalene, 1,5-dihydroxy	1.6×10^6	CD_3OD	k_r	180	135
Naphthalene, 1,6-dihydroxy	1.2×10^6	CD_3OD	k_r	240	180
Naphthalene, 1,7-dihydroxy	6.8×10^5	CD_3OD	k_r	424	317
Naphthalene, 1,8-dihydroxy	3.0×10^7	CD_3OD	k_r	9.6	7.2
Furan	8.9×10^6	Methanol	k_r	32.4	24.2
Furan, 2,5-bis(4-methoxyphenyl)	9.9×10^7	CH_2Cl_2	k_d	2.9	2.2
Aniline	2.0×10^9	Methanol	k_d	0.1	0.1
2-Ethyl-1,3-butadiene	7.2×10^4	$CHCl_3$	k_d	4007	2994
Cyclopentadiene	1.0×10^8	$CHCl_3$	k_d	2.9	2.2
Pyridine	2.0×10^3	CCl_4	k_d	144 237	107 784
Pyridinium, 1-methyl	6.5×10^5	D_2O	k_d	444	332
Pyridine, 3,5-dicarboxylic acid, 1,4-dihydro-2,6-dimethyl-dicyclohexyl ester	6.0×10^6	$CHCl_3$	k_d	48.1	35.9
1,4-Dihydro-2,6-dimethyl-4-(2-nitrophenyl)-3,5-pyridine-dicarboxylic acid dimethyl ester (nifedipine)	3.8×10^4 [e]	Ethanol	k_r	7591	5673
1,4-Dihydro-2,6-dimethyl-4-(3-nitrophenyl)-3,5-pyridine-dicarboxylic acid ethyl methyl ester (nitrendipine)	9.7×10^4 [e]	Ethanol	k_r	2974	2222
Benzoic acid, 2-hydroxy-methyl ester	1.6×10^8	H_2O pH 10	k_r	1.8	1.3
Indole	7.0×10^7	H_2O pH 7.2	k_d	4.1	3.1
Indole-3-acetate ion	9.2×10^7	H_2O pH 7	k_r	3.1	2.3
Indole-3-carboxylate ion	1.4×10^7	H_2O pH 7	k_r	20.6	15.4
Quinoline	$\leq 1.0 \times 10^9$	EtOH	k_d	$\geq$0.3	$\geq$0.2
Quinoline, 8-hydroxy	1.1×10^8	$CHCl_3$	k_d	2.6	2.0

[a] Data from Wilkinson *et al.*[77] except otherwise mentioned. [b] Solvent used in the second-order rate constant measurement. [c] k_r is the reactive rate constant while k_d is the rate constant for the deactivation of singlet oxygen (see text). [d] Corresponding $[^1O_2]_{ss}$ are 6.67 and 8.89×10^{-13} M for SMC and BHC, respectively. [e] Data from Pizarro-Urzua *et al.*[83]

literature observations that aromatic DBC is more sensitive that the bulk DOM to photoirradiation.

Overall, this kinetic analysis suggests that indirect phototransformation induced by $^1O_2$ and ^{3}DOM* may explain the fast decrease in absorbance for the wildfire ash extracts under sunlight irradiation.

4. Conclusion

Wildfire-affected watersheds can introduce significant amounts of wildfire-impacted DOM into streams, impacting both the natural ecosystem and the engineered systems that rely on this water source. For example, an increase in disinfection byproduct formation potential has been shown for wildfire-impacted water.[90] This work showed that DOM has optical and photochemical properties, such as higher $\Phi_{^1O_2}$, Φ_F, and SUVA, distinct of non-impacted DOM. Upon photoirradiation, these properties begin to resemble those of non-impacted and unirradiated DOM. At a watershed level, this may correspond to a scenario where the wildfire-impacted DOM signal is visible and significant near the burned area, but decreases downstream, due to photobleaching and dilution. The average molecular weight of the wildfire-impacted DOM is lower than the non-impacted DOM, which may be the reason for the observed decrease in coagulability of wildfire-impacted DOM.[90] Upon photoirradiation, the lower average molecular weight should be conserved and only affected by dilution. This differs from the optical properties that are also affected by photoirradiation, and the lower average molecular weight should be detectable further downstream of the wildfire impacted area than the change of optical properties. Wildfire-impacted DOM was shown to be sensitive to photobleaching and efficiently photomineralized to CO_2, which raises the question of DOM stability post wildfire, and how long would it take for wildfire-impacted DOM to resemble that of non-impacted sources.

Data availability

The data supporting this article have been included as part of the ESI.†

Conflicts of interest

The authors declare no competing financial interest.

Acknowledgements

The authors would like to thank the USDA-Forest Service Rocky Mountain Biogeochemical Station for their assistance collecting samples and providing field details of ash collection. We also thank Leah Rivera and Blair Hanson for their assistance with laboratory experiments.

References

1 S. A. Parks, C. Miller, M.-A. Parisien, L. M. Holsinger, S. Z. Dobrowski and J. Abatzoglou, Wildland fire deficit and surplus in the western United States, 1984–2012, *Ecosphere*, 2015, **6**(12), 1–13.
2 D. Bowman, C. A. Kolden, J. T. Abatzoglou, F. H. Johnston, G. R. van der Werf and M. Flannigan, Vegetation fires in the anthropocene, *Nat. Rev. Earth Environ.*, 2020, **1**(10), 500–515.
3 A. M. Lopez, C. C. E. Avila, J. P. Vanderroest, H. K. Roth, S. Fendorf and T. Borch, Molecular insights and impacts of wildfire-induced soil chemical changes, *Nat. Rev. Earth Environ.*, 2024, **5**, 431–446.
4 J. T. Abatzoglou and A. P. Williams, Impact of anthropogenic climate change on wildfire across western US forests, *Proc. Natl. Acad. Sci. U. S. A.*, 2016, **113**(42), 11770–11775.
5 J.-J. Wang, R. A. Dahlgren and A. T. Chow, Controlled burning of forest detritus altering spectroscopic characteristics and chlorine reactivity of dissolved organic matter: Effects of temperature and oxygen availability, *Environ. Sci. Technol.*, 2015, **49**(24), 14019–14027.
6 A. K. Hohner, L. G. Terry, E. B. Townsend, R. S. Summers and F. L. Rosario-Ortiz, Water treatment process evaluation of wildfire-affected sediment leachates, *Environ. Sci.: Water Res. Technol.*, 2017, **3**(2), 352–365.
7 K. M. Cawley, A. K. Hohner, D. C. Podgorski, W. T. Cooper, J. A. Korak and F. L. Rosario-Ortiz, Molecular and spectroscopic characterization of water extractable organic matter from thermally altered soils reveal insight into disinfection byproduct precursors, *Environ. Sci. Technol.*, 2017, **51**(2), 771–779.
8 L. Thuile Bistarelli, C. Poyntner, C. Santin, S. H. Doerr, M. V. Talluto, G. Singer and G. Sigmund, Wildfire-derived pyrogenic carbon modulates riverine organic matter and biofilm enzyme activities in an *in situ* flume experiment, *ACS ES&T Water*, 2021, **1**(7), 1648–1656.
9 D. P. Pompeani, K. K. McLauchlan, B. V. Chileen, W. J. Calder, B. N. Shuman and P. E. Higuera, The biogeochemical consequences of late holocene wildfires in three subalpine lakes from northern Colorado, *Quat. Sci. Rev.*, 2020, **236**, 106293.
10 R. Sanchez, T. Meixner, T. Roy, P. Ferre, M. Whitaker and J. Chorover, Physical and biogeochemical drivers of solute mobilization and flux through the critical zone after wildfire, *Front. Water*, 2023, **5**, 1148298.
11 A. S. Wozniak, S. Mitra, A. I. Goranov, A. R. Zimmerman, K. W. Bostick and P. G. Hatcher, Effects of environmental aging on wildfire particulate and dissolved pyrogenic organic matter characteristics, *ACS Earth Space Chem.*, 2024, **8**(1), 104–118.
12 S. Zhu, P. Yang, Y. Yin, S. Zhang, J. Lv, S. Tian, T. Jiang and D. Wang, Influences of wildfire on the soil dissolved organic matter characteristics and its electron-donating capacity, *Water Res.*, 2024, **266**, 122382.
13 A. K. Hohner, K. Cawley, J. Oropeza, R. S. Summers and F. L. Rosario-Ortiz, Drinking water treatment response following a Colorado wildfire, *Water Res.*, 2016, **105**, 187–198.
14 G. McKay, A. K. Hohner and F. L. Rosario-Ortiz, Use of optical properties for evaluating the presence of pyrogenic

organic matter in thermally altered soil leachates, *Environ. Sci.: Processes Impacts*, 2020, **22**(4), 981–992.
15 S. F. Murphy, J. H. Writer, R. B. McCleskey and D. A. Martin, The role of precipitation type, intensity, and spatial distribution in source water quality after wildfire, *Environ. Res. Lett.*, 2015, **10**(8), 084007.
16 H. G. Smith, G. J. Sheridan, P. N. J. Lane, P. Nyman and S. Haydon, Wildfire effects on water quality in forest catchments: A review with implications for water supply, *Hydrology*, 2011, **396**(1–2), 170–192.
17 C. M. Preston and M. W. I. Schmidt, Black (pyrogenic) carbon: A synthesis of current knowledge and uncertainties with special consideration of boreal regions, *Biogeosciences*, 2006, **3**(4), 397–420.
18 W. Bahureksa, R. B. Young, A. M. McKenna, H. Chen, K. A. Thorn, F. L. Rosario-Ortiz and T. Borch, Nitrogen enrichment during soil organic matter burning and molecular evidence of Maillard reactions, *Environ. Sci. Technol.*, 2022, **56**(7), 4597–4609.
19 E. K. Coward, K. Seech, M. L. Carter, R. E. Flick and V. H. Grassian, Of sea and smoke: Evidence of marine dissolved organic matter deposition from 2020 western United States wildfires, *Environ. Sci. Technol. Lett.*, 2022, **9**(10), 869–876.
20 S. J. Fischer, T. S. Fegel, P. J. Wilkerson, L. Rivera, C. C. Rhoades and F. L. Rosario-Ortiz, Fluorescence and absorbance indices for dissolved organic matter from wildfire ash and burned watersheds, *ACS ES&T Water*, 2023, **3**(8), 2199–2209.
21 C. Ward, R. Sleighter, P. Hatcher and R. Cory, Insights into the complete and partial photooxidation of black carbon in surface waters, *Environ. Sci.: Processes Impacts*, 2014, **16**, 721–731.
22 K. Bostick, A. Zimmerman, A. Goranov, S. Mitra, P. Hatcher and A. Wozniak, Photolability of pyrogenic dissolved organic matter from a thermal series of laboratory -prepared chars, *Sci. Total Environ.*, 2020, **724**, 138198.
23 H. Wang and H. Zhou, Insights into the role of photobleaching on the photophysical and photochemical properties of dissolved black carbon, *ACS ES&T Water*, 2024, **4**, 2225–2234.
24 S. Wagner and R. Jaffé, Effect of photodegradation on molecular size distribution and quality of dissolved black carbon, *Org. Geochem.*, 2015, **86**, 1–4.
25 Y. Chen, K. Sun, H. Sun, Y. Yang, Y. Li, B. Gao and B. Xing, Photodegradation of pyrogenic dissolved organic matter increases bioavailability: Novel insight into bioalteration, microbial community succession, and c and n dynamics, *Chem. Geol.*, 2022, **605**, 120964.
26 A. Goranov, A. Wozniak, K. Bostick, A. Zimmerman, S. Mitra and P. Hatcher, Photochemistry after fire: Structural transformations of pyrogenic dissolved organic matter elucidated by advanced analytical techniques, *Geochim. Cosmochim. Acta*, 2020, **290**, 271–292.
27 X. Zuo, Z. Ouyang, J. Liao, R. Ding, W. Zhang, C. Zhang, X. Guo and L. Zhu, Novel insights into the relationship between the functional groups and photoactivity of biochar-derived dissolved organic matter, *Water Res.*, 2024, **260**, 121892.
28 K. McNeill and S. Canonica, Triplet state dissolved organic matter in aquatic photochemistry: Reaction mechanisms, substrate scope, and photophysical properties, *Environ. Sci.: Processes Impacts*, 2016, **18**, 1381–1399.
29 X. Z. Niu, C. Liu, L. Gutierrez and J. P. Croué, Photobleaching-induced changes in photosensitizing properties of dissolved organic matter, *Water Res.*, 2014, **66**, 140–148.
30 J. E. Grebel, J. J. Pignatello, W. H. Song, W. J. Cooper and W. A. Mitch, Impact of halides on the photobleaching of dissolved organic matter, *Mar. Chem.*, 2009, **115**(1–2), 134–144.
31 F. Leresche, J. R. Salazar, D. J. Pfotenhauer, M. P. Hannigan, B. J. Majestic and F. L. Rosario-Ortiz, Photochemical aging of atmospheric particulate matter in the aqueous phase, *Environ. Sci. Technol.*, 2021, **55**(19), 13152–13163.
32 S. Buckley, F. Leresche, K. Norris and F. Rosario-Ortiz, Role of direct and sensitized photolysis in the photomineralization of dissolved organic matter and model chromophores to carbon dioxide, *Environ. Sci. Technol.*, 2024, **58**(31), 13808–13819.
33 D. Wan, H. Y. Wang, V. K. Sharma, S. Selvinsimpson, H. L. Dai, F. Luo, C. J. Wang and Y. Chen, Mechanistic investigation of enhanced photoreactivity of dissolved organic matter after chlorination, *Environ. Sci. Technol.*, 2021, **55**(13), 8937–8946.
34 F. Leresche, G. McKay, T. Kurtz, U. von Gunten, S. Canonica and F. L. Rosario-Ortiz, Effects of ozone on the photochemical and photophysical properties of dissolved organic matter, *Environ. Sci. Technol.*, 2019, **53**(10), 5622–5632.
35 M. Li, F. X. Bao, Y. Zhang, H. Sheng, C. C. Chen and J. C. Zhao, Photochemical aging of soot in the aqueous phase: Release of dissolved black carbon and the formation of $^1O_2$, *Environ. Sci. Technol.*, 2019, **53**(21), 12311–12319.
36 H. Wang, H. X. Zhou, J. Z. Ma, J. X. Nie, S. W. Yan and W. H. Song, Triplet photochemistry of dissolved black carbon and its effects on the photochemical formation of reactive oxygen species, *Environ. Sci. Technol.*, 2020, **54**(8), 4903–4911.
37 H. Y. Fu, H. T. Liu, J. D. Mao, W. Y. Chu, Q. L. Li, P. J. J. Alvarez, X. L. Qu and D. Q. Zhu, Photochemistry of dissolved black carbon released from biochar: Reactive oxygen species generation and phototransformation, *Environ. Sci. Technol.*, 2016, **50**(3), 1218–1226.
38 F. Lian, Y. K. Zhang, S. G. Gu, Y. R. Han, X. S. Cao, Z. Y. Wang and B. S. Xing, Photochemical transformation and catalytic activity of dissolved black nitrogen released from environmental black carbon, *Environ. Sci. Technol.*, 2021, **55**(9), 6476–6484.
39 Y. L. Wang, B. B. Wu, X. S. Zheng, B. L. Chen and C. H. Chu, Assessing the quantum yield spectrum of photochemically produced reactive intermediates from black carbon of

various sources and properties, *Water Res.*, 2023, **229**, 119450.
40 M. Madhiyan and K. J. Moor, Singlet oxygen quantum yields of pyrogenic dissolved organic matter from lab-prepared and wildfire chars, *Environ. Sci. Technol.*, 2023, **58**(2), 1265–1273.
41 L. Li, W. Cheng, X. Xie, R. Zhao, Y. Wang and Z. Wang, Photo-reactivity of dissolved black carbon unveiled by combination of optical spectroscopy and FT-ICR MS analysis: Effects of pyrolysis temperature, *Water Res.*, 2024, **251**(1), 121138.
42 B. Hanson, U. Wünsch, S. Buckley, S. Fischer, F. Leresche, K. Murphy, J. D'Andrilli and F. L. Rosario-Ortiz, DOM molecular weight fractionation and fluorescence quantum yield assessment using a coupled in-line sec optical property system, *ACS ES&T Water*, 2022, **2**(12), 2491–2501.
43 M. Bodí, D. Martin, V. Balfour, C. Santín, S. Doerr, P. Pereira, A. Cerdà and J. Mataix-Solera, Wild land fire ash: Production, composition and eco-hydro-geomorphic effects, *Earth-Sci. Rev.*, 2014, **130**, 103–127.
44 R. S. Gabor, M. A. Burns, R. H. Lee, J. B. Elg, C. J. Kemper, H. R. Barnard and D. M. McKnight, Influence of leaching solution and catchment location on the fluorescence of water-soluble organic matter, *Environ. Sci. Technol.*, 2015, **49**(7), 4425–4432.
45 F. Leresche, J. A. Torres-Ruiz, T. Kurtz, U. von Gunten and F. L. Rosario-Ortiz, Optical properties and photochemical production of hydroxyl radical and singlet oxygen after ozonation of dissolved organic matter, *Environ. Sci.: Water Res. Technol.*, 2021, **7**(2), 346–356.
46 E. Appiani, R. Ossola, D. E. Latch, P. R. Erickson and K. McNeill, Aqueous singlet oxygen reaction kinetics of furfuryl alcohol: Effect of temperature, ph, and salt content, *Environ. Sci.: Processes Impacts*, 2017, **19**(4), 507–516.
47 R. Ossola, O. M. Jonsson, K. Moor and K. McNeill, Singlet oxygen quantum yields in environmental waters, *Chem. Rev.*, 2021, **121**(7), 4100–4146.
48 T. Dittmar, B. Koch, N. Hertkorn and G. Kattner, A simple and efficient method for the solid-phase extraction of dissolved organic matter (spe-dom) from seawater, *Limnol. Oceanogr.: Methods*, 2008, **6**, 230–235.
49 S. Buckley, F. Leresche, B. Hanson and F. L. Rosario-Ortiz, Decoupling optical response and photochemical formation of singlet oxygen in size isolated fractions of ozonated dissolved organic matter, *Environ. Sci. Technol.*, 2023, **57**(14), 5603–5610.
50 G. McKay, J. A. Korak, P. R. Erickson, D. E. Latch, K. McNeill and F. L. Rosario-Ortiz, The case against charge transfer interactions in dissolved organic matter photophysics, *Environ. Sci. Technol.*, 2018, **52**(2), 406–414.
51 S. J. Blanksby and G. B. Ellison, Bond dissociation energies of organic molecules, *Acc. Chem. Res.*, 2003, **36**(4), 255–263.
52 M. I. de Heer, H. G. Korth and P. Mulder, Poly methoxy phenols in solution: O-H bond dissociation enthalpies, structures, and hydrogen bonding, *Org. Chem.*, 1999, **64**(19), 6969–6975.
53 G. Certini, Effects of fire on properties of forest soils: A review, *Oecologia*, 2005, **143**, 1–10.
54 R. Cundall and L. Pereira, Temperature and solvent effects on fluorescence of some simple aromatic molecules, *J. Chem. Soc., Faraday Trans. 2*, 1972, (68), 1152–1163.
55 C. Parker and T. Joyce, Determination of triplet formation efficiencies by measurement of sensitized delayed fluorescence, *Trans. Faraday Soc.*, 1966, **62**, 2785–2792.
56 J. Peuravuori and K. Pihlaja, Molecular size distribution and spectroscopic properties of aquatic humic substances, *Anal. Chim. Acta*, 1997, **337**(2), 133–149.
57 A. C. Maizel and C. K. Remucal, Molecular composition and photochemical reactivity of size-fractionated dissolved organic matter, *Environ. Sci. Technol.*, 2017, **51**(4), 2113–2123.
58 G. McKay, W. X. Huang, C. Romera-Castillo, J. E. Crouch, F. L. Rosario-Ortiz and R. Jaffé, Predicting reactive intermediate quantum yields from dissolved organic matter photolysis using optical properties and antioxidant capacity, *Environ. Sci. Technol.*, 2017, **51**(10), 5404–5413.
59 R. M. Dalrymple, A. K. Carfagno and C. M. Sharpless, Correlations between dissolved organic matter optical properties and quantum yield of singlet oxygen and hydrogen peroxide, *Environ. Sci. Technol.*, 2010, **44**, 5824–5829.
60 R. Du, J. Wen, J. Huang, Q. Zhang, X. Shi, B. Wang, S. Deng and G. Yu, Dissolved organic matter isolates obtained by solid phase extraction exhibit higher absorption and lower photo-reactivity: Effect of components, *Water Res.*, 2024, **256**, 121604.
61 K. Sekimoto, A. R. Koss, J. B. Gilman, V. Selimovic, M. M. Coggon, K. J. Zarzana, B. Yuan, B. M. Lerner, S. S. Brown, C. Warneke, R. J. Yokelson, J. M. Roberts and J. de Gouw, High- and low-temperature pyrolysis profiles describe volatile organic compound emissions from western US wildfire fuels, *Atmos. Chem. Phys.*, 2018, **18**(13), 9263–9281.
62 J. R. Helms, J. D. Mao, A. Stubbins, K. Schmidt-Rohr, R. G. M. Spencer, P. J. Hernes and K. Mopper, Loss of optical and molecular indicators of terrigenous dissolved organic matter during long-term photobleaching, *Aquat. Sci.*, 2014, **76**(3), 353–373.
63 R. Del Vecchio and N. V. Blough, Photobleaching of chromophoric dissolved organic matter in natural waters: Kinetics and modeling, *Mar. Chem.*, 2002, **78**(4), 231–253.
64 S.-A. Li, Q. Wang, H. Ma, X. Cao, Y. Song, F. Cui and A. J. Tanentzap, Photochemical processes transform dissolved organic matter differently depending on its initial composition, *Sci. Total Environ.*, 2024, **923**, 171465.
65 A. D. Holt, A. M. Kellerman, W. B. Li, A. Stubbins, S. Wagner, A. McKenna, J. Fellman, E. Hood and R. G. M. Spencer, Assessing the role of photochemistry in driving the composition of dissolved organic matter in glacier runoff, *J. Geophys. Res.:Biogeosci.*, 2021, **126**(12), e2021JG006516.
66 M. Gonsior, B. M. Peake, W. T. Cooper, D. Podgorski, J. D'Andrilli and W. J. Cooper, Photochemically induced changes in dissolved organic matter identified by ultrahigh

resolution Fourier transform ion cyclotron resonance mass spectrometry, *Environ. Sci. Technol.*, 2009, **43**(3), 698–703.

67 E. M. Thurman, Y. Yu, I. Ferrer, K. A. Thorn and F. L. Rosario-Ortiz, Molecular identification of water-extractable organic carbon from thermally heated soils: C-13 NMR and accurate mass analyses find benzene and pyridine carboxylic acids, *Environ. Sci. Technol.*, 2020, **54**(5), 2994–3001.

68 I. Ferrer, E. M. Thurman, J. A. Zweigenbaum, S. F. Murphy, J. P. Webster and F. L. Rosario-Ortiz, Wildfires: Identification of a new suite of aromatic polycarboxylic acids in ash and surface water, *Sci. Total Environ.*, 2021, **770**, 144661.

69 E. M. Thurman, I. Ferrer, M. Bowden, C. Mansfeldt, T. S. Fegel, C. C. Rhoades and F. Rosario-Ortiz, Occurrence of benzene polycarboxylic acids in ash and streamwater after the cameron peak fire, *ACS ES&T Water*, 2023, **3**(12), 3848–3857.

70 H. X. Xie, O. C. Zafiriou, W. J. Cai, R. G. Zepp and Y. C. Wang, Photooxidation and its effects on the carboxyl content of dissolved organic matter in two coastal rivers in the southeastern united states, *Environ. Sci. Technol.*, 2004, **38**(15), 4113–4119.

71 C. P. Ward and R. M. Cory, Complete and partial photo-oxidation of dissolved organic matter draining permafrost soils, *Environ. Sci. Technol.*, 2016, **50**(7), 3545–3553.

72 A. Stubbins, J. Niggemann and T. Dittmar, Photo-lability of deep ocean dissolved black carbon, *Biogeosci*, 2012, **9**(5), 1661–1670.

73 D. Budac and P. Wan, Photodecarboxylation - mechanism and synthetic utility, *J. Photochem. Photobiol., A*, 1992, **67**(2), 135–166.

74 Z. Najminejad, Oxidative decarboxylation of arylacetic acids and arylacetic esters with singlet molecular oxygen generated from trans-5-hydroperoxy-3,5-dimethyl-1,2-dioxolan-3-yl ethaneperoxate, *J. Chem. Sci.*, 2024, **136**(11), DOI: 10.1007/s12039-023-02243-5.

75 J. R. Helms, A. Stubbins, J. D. Ritchie, E. C. Minor, D. J. Kieber and K. Mopper, Absorption spectral slopes and slope ratios as indicators of molecular weight, source, and photobleaching of chromophoric dissolved organic matter, *Limnol. Oceanogr.*, 2008, **53**(3), 955–969.

76 K. McNeill and S. Canonica, Triplet state dissolved organic matter in aquatic photochemistry: Reaction mechanisms, substrate scope, and photophysical properties, *Environ. Sci.: Processes Impacts*, 2016, **18**, 1381–1399.

77 F. Wilkinson, W. P. Helman and A. B. Ross, Rate constants for the decay and reactions of the lowest electronically excited singlet-state of molecular-oxygen in solution - an expanded and revised compilation, *J. Phys. Chem. Ref. Data*, 1995, **24**(2), 663–1021.

78 T. Zeng and W. A. Arnold, Pesticide photolysis in prairie potholes: Probing photosensitized processes, *Environ. Sci. Technol.*, 2013, **47**(13), 6735–6745.

79 A. L. Boreen, W. A. Arnold and K. McNeill, Triplet-sensitized photodegradation of sulfa drugs containing six-membered heterocyclic groups: Identification of an SO_2 extrusion photoproduct, *Environ. Sci. Technol.*, 2005, **39**(10), 3630–3638.

80 W. R. Haag, J. Hoigné, E. Gassman and A. M. Braun, Singlet oxygen in surface waters. 1. Furfuryl alcohol as a trapping agent, *Chemosphere*, 1984, **13**(5–6), 631–640.

81 R. M. Cory, K. McNeill, J. P. Cotner, A. Amado, J. M. Purcell and A. G. Marshall, Singlet oxygen in the coupled photochemical and biochemical oxidation of dissolved organic matter, *Environ. Sci. Technol.*, 2010, **44**(10), 3683–3689.

82 R. M. Cory, J. B. Cotner and K. McNeill, Quantifying interactions between singlet oxygen and aquatic fulvic acids, *Environ. Sci. Technol.*, 2009, **43**(3), 718–723.

83 N. A. Pizarro-Urzua and L. J. Nunez-Vergara, Nifedipine and nitrendipine reactivity toward singlet oxygen, *J. Photochem. Photobiol., A*, 2005, **175**(2–3), 129–137.

84 D. E. Latch and K. McNeill, Microheterogeneity of singlet oxygen distributions in irradiated humic acid solutions, *Science*, 2006, **311**(5768), 1743–1747.

85 M. Grandbois, D. E. Latch and K. Mcneill, Microheterogeneous concentrations of singlet oxygen in natural organic matter isolate solutions, *Environ. Sci. Technol.*, 2008, **42**(24), 9184–9190.

86 H. Wang, M. Han, M. Wang and H. Zhou, Microheterogeneous triplet oxidation of hydrophobic organic contaminants in dissolved black carbon solutions under simulated solar irradiation, *Environ. Sci. Technol.*, 2022, **56**(20), 14574–14584.

87 S. W. Yan, J. Q. Sun, H. T. Sha, Q. Li, J. X. Nie, J. M. Zou, C. H. Chu and W. H. Song, Microheterogeneous distribution of hydroxyl radicals in illuminated dissolved organic matter solutions, *Environ. Sci. Technol.*, 2021, **55**(15), 10524–10533.

88 P. R. Erickson, N. Walpen, J. J. Guerard, S. N. Eustis, J. S. Arey and K. McNeill, Controlling factors in the rates of oxidation of anilines and phenols by triplet methylene blue in aqueous solution, *J. Phys. Chem. A*, 2015, **119**(13), 3233–3243.

89 F. Leresche, L. Ludvíková, D. Heger, P. Klán, U. von Gunten and S. Canonica, Laser flash photolysis study of the photoinduced oxidation of 4-(dimethylamino)benzonitrile (DMABN), *Photochem. Photobiol. Sci.*, 2019, **18**(2), 534–545.

90 J. H. Writer, A. Hohner, J. Oropeza, A. Schmidt, K. Cawley and F. L. Rosario-Ortiz, Water treatment implications after the High Park wildfire in Colorado, *J. - Am. Water Works Assoc.*, 2014, **106**(4), E189–E199.